Memristive and neuromorphic behavior in a Li x CoO 2 nanobattery

V H Mai, A. Moradpour, P. Auban Senzier, C Pasquier, K Wang, M. J.
Rozenberg, J. Giapintzakis, C N Mihailescu, C M Ortanidou, E Svoukis, et al.

OPEN

Memristive and neuromorphic behavior in a Li$_x$CoO$_2$ nanobattery

V. H. Mai[1,2], A. Moradpour[3], P. Auban Senzier[3], C. Pasquier[3], K. Wang[3], M. J. Rozenberg[3,4], J. Giapintzakis[5], C. N. Mihailescu[5], C. M. Orfanidou[5], E. Svoukis[5], A. Breza[5,6], Ch B. Lioutas[6], S. Franger[7], A. Revcolevschi[7], T. Maroutian[2], P. Lecoeur[2], P. Aubert[2], G. Agnus[2], R. Salot[8], P. A. Albouy[3], R. Weil[3], D. Alamarguy[1], K. March[3], F. Jomard[9], P. Chrétien[1] & O. Schneegans[1]

[1]Laboratoire de Génie Électrique de Paris, CNRS-UMR 8507, Universités UPMC et Paris-Sud, Supélec, F-91192 Gif-sur-Yvette, France, [2]Institut d'Électronique Fondamentale, CNRS-UMR 8622, Université Paris-Sud, 91405 Orsay, France, [3]Laboratoire de Physique des Solides, CNRS-UMR 8502, Université Paris-Sud, F-91405 Orsay, France, [4]Departamento de Física Juan José Giambiagi, FCEN, Universidad de Buenos Aires, Ciudad Universitaria, Pabellón I, (1428) Buenos Aires, Argentina, [5]Nanotechnology Research Center and Department of Mechanical and Manufacturing Engineering, University of Cyprus, 1678 Nicosia, Cyprus, [6]Physics Department, Aristotle University of Thessaloniki, GR-54124, Thessaloniki, Greece, [7]Laboratoire de Physico-Chimie de l'Etat Solide, CNRS-UMR 8182, Université Paris-Sud, F-91405 Orsay, France, [8]Liten-CEA de Grenoble, F-38054 Grenoble, France, [9]Groupe d'Etude de la Matière Condensée, CNRS-UMR 8635, Université de Versailles Saint-Quentin-En-Yvelines, F-78035 Versailles, France.

The phenomenon of resistive switching (RS), which was initially linked to non-volatile resistive memory applications, has recently also been associated with the concept of memristors, whose adjustable multilevel resistance characteristics open up unforeseen perspectives in cognitive computing. Herein, we demonstrate that the resistance states of Li$_x$CoO$_2$ thin film-based metal-insulator-metal (MIM) solid-state cells can be tuned by sequential programming voltage pulses, and that these resistance states are dramatically dependent on the pulses input rate, hence emulating biological synapse plasticity. In addition, we identify the underlying electrochemical processes of RS in our MIM cells, which also reveal a nanobattery-like behavior, leading to the generation of electrical signals that bring an unprecedented new dimension to the connection between memristors and neuromorphic systems. Therefore, these Li$_x$CoO$_2$-based MIM devices allow for a combination of possibilities, offering new perspectives of usage in nanoelectronics and bio-inspired neuromorphic circuits.

The current interest in the field of resistive switching (RS) materials[1–4] has recently been amplified largely by an enlightening re-investigation of TiO$_2$ film devices[5] connecting RS[6] to the concept of memory resistors (memristors). This remarkable connection has highlighted mainly the non-volatile adjustable (multilevel) resistance characteristics of these devices, and has widened the considered applications of RS further than those previously which were limited to non-volatile memories based on binary modifications involving exclusively two switching resistance states. Moreover, the realization of bio-inspired neuromorphic circuits, based on the present fragmentary knowledge of the brain, became viable considering possible emulations of the plasticity of biological synapses by the dynamic pulse-induced behavior of memristors[5,7]. This synapse-like learning ability, which opens unforeseen perspectives in the field of cognitive computing, has recently been investigated including devices based on Ag and Cu atomic switches[8–10], perovskites[11], titanium[12] and tungsten oxide[13] film devices, and phase change materials[14].

Li$_x$CoO$_2$ is widely used as a cathode material in current rechargeable lithium batteries. Beyond this, the occurrence of bipolar RS phenomena has been recently observed for the first time, using a metal/insulator/metal (MIM) solid-state cell containing this layered mixed-valence cobalt oxide[15]. Here, we establish that the resistance states of the MIM devices are tunable between two extreme values, using repetitive voltage pulses over a threshold value. We also find that the different resistance states are dramatically dependent on the input rate of non-overlapping pulses, which is a dynamical effect similar to temporal summations of action potentials[16] and reminiscent of the frequency-dependent connectivity of the synapses[17]. Beyond these attractive pulse-related features emulating biological synapse plasticity, we find that the system investigated here reveals *both* the existence of RS and the occurrence of a battery-like voltage, and we identify the specific electrochemical processes for these interconnected phenomena. Our devices, therefore, bring together the emulation of a biological synapse,

and also an additional feature involving the occurrence of a significant electromotive force that results in the generation of electrical signals, which are more specific of a neuron. Remarkably, new insights into nanoionic-type memristive cells are coming into focus[18].

Results

We have recently demonstrated[15] the occurrence of large bipolar RS phenomena in MIM {Au/Li$_x$CoO$_2$/doped-Si} devices, which however exhibited only two resistance states: R$_{OFF}$ (which corresponds to both the resistance of the pristine cell, and the highest resistance after voltage cycling) and R$_{ON}$ (lowest resistance state), with a R$_{OFF}$/R$_{ON}$ ratio in the range 10^4–10^5. Here, we establish the multilevel character of this RS in MIM cells (schematic view illustrated in Fig. 1a) containing Li$_x$CoO$_2$ thin films (whose structure is shown in Fig. 1b and 1c). Indeed, as an example shown in Fig. 1d, four well-separated stable resistance states are observed, thus clearly pointing out high multilevel resistance tuning possibilities for such devices.

Furthermore, due to their cumulative response to excitations[7,8,14,19], memristive devices are promising candidates in the field of cognitive computation[5,7], allowing learning rules such as Spike-Timing Dependent Plasticity (STDP). Such biological synapse-like behavior is of crucial importance towards the realization of neuro-morphic systems[11]. In this respect, we first establish the MIM cells conductance evolution -reflecting the synaptic weight change- by sequential programming pulses. Below a negative threshold value (about -3 V), successive substrate/tip voltage pulses of negative polarity yield a several decades conductance increase with the number of pulses (red plots in Fig. 1e). Subsequent pulses of positive polarity yield back a conductance decrease (blue plots in Fig. 1e), thus highlighting the memristive additive behavior of the films. Then, in a second step, we investigated the synapses plasticity as a function of the stimulation rate. This is measured through the evolution of the current ratio i_{fin}/i_{init} between the current measured after (i_{fin}) and before (i_{init}) twenty non-overlapping pulses, applied at different frequencies, f. Fig. 1f clearly shows a strong frequency-dependent behavior, with the i_{fin}/i_{init} ratio ranging from 2 up to 10^3.

These observations and the importance of their potential application, require a better understanding of the underlying electrochemical mechanisms that govern such a behavior. In this respect, we first discuss the issue of filamentary vs homogeneous RS, which is very important, as a better downscaling may be achieved in the case of a homogeneous RS[20,21]. As Li$_x$CoO$_2$ is largely used in lithium ion batteries, an "homogeneous" switching would be likely. To demonstrate this point, we introduce a new original method of investigation that involves measuring the decrease in the MIM cells resistance from the
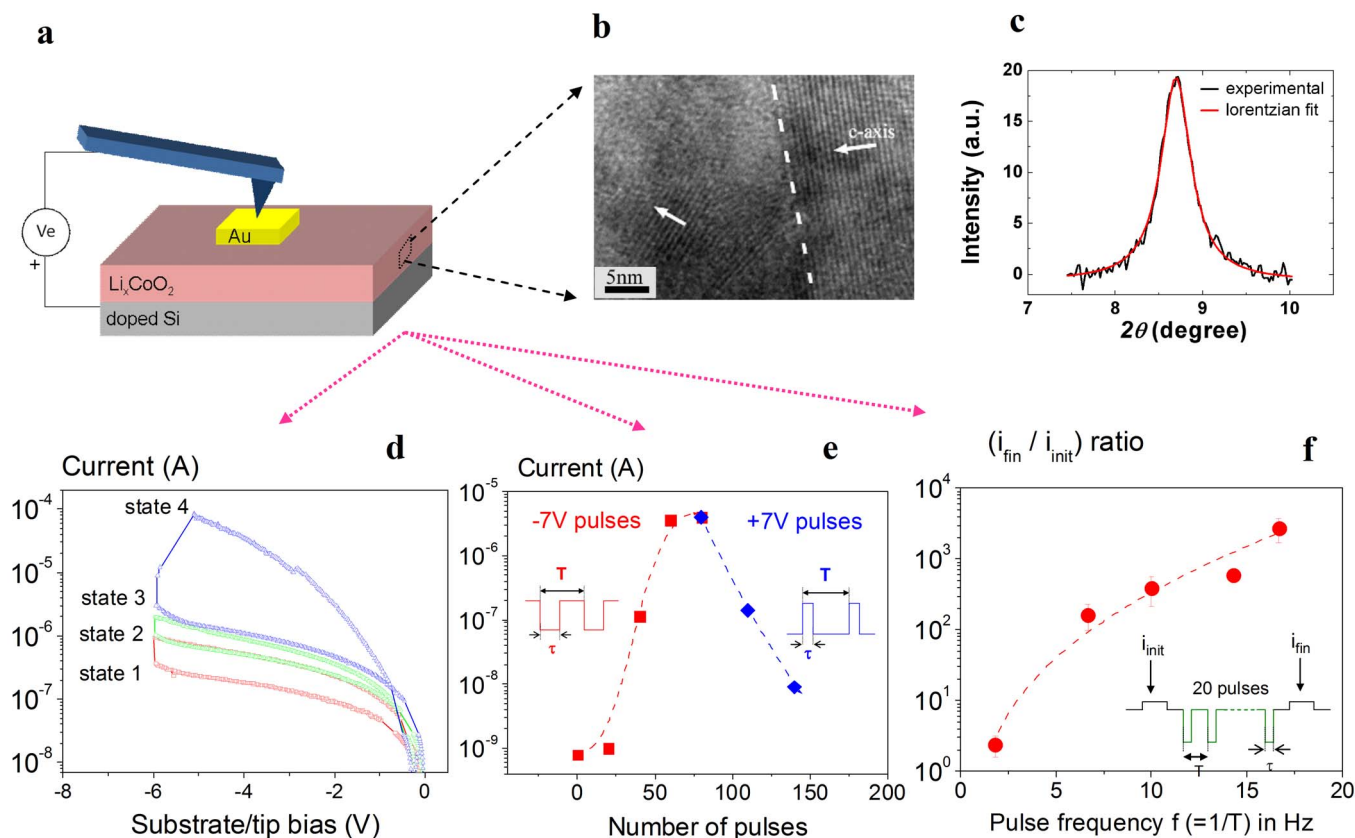

Figure 1 | Schematic diagram of a Li$_x$CoO$_2$-based MIM cell, structural characteristics of a Li$_x$CoO$_2$ film, and behavior of MIM cells under different kinds of action potentials. (a) Schematic diagram of a typical M/Li$_x$CoO$_2$/M cell (30×30 μm^2 for d, e and f). The probe/upper electrode contact resistance is in the 10^3–10^4 Ω range, which is low, compared to the MIM resistance. (b) Bright-Field cross-section transmission electron microscopy (TEM) image of a Li$_x$CoO$_2$ film, exhibiting a mean c-axis direction nearly parallel to the substrate surface. (c) X-ray diffraction profile of the (003) reflection for a Li$_x$CoO$_2$ film. The c-parameter value derived from the peak position is 1.408 nm that points to a stoichiometry x = 0.95 (see Methods). (d) Lower/upper electrode successive I–V curves ($0 \rightarrow -6V \rightarrow 0$ voltage ramps, 3 V.s^{-1} sweeping rate); the first (in red) and the second (in green) curves include a 1 s waiting time period at -6 V; the third curve (in blue) includes a 2 s waiting time at -6 V. Four well-separated resistance states can be observed here. (e) The conductance of MIM cells (current measured at $+1$ V) increases after each consecutive set of 20 negative pulses of -7 V ($\tau = 50$ ms, T = 100 ms, in red) and decreases after each consecutive set of 30 positive pulses of $+7$ V ($\tau = 10$ ms, T = 100 ms, in blue) (f) the MIM conductance has been measured (at $+1$ V) before (i_{init}) and after (i_{fin}) 20 non-overlapping pulses (-7 V, $\tau = 50$ ms); the corresponding ratio i_{fin}/i_{init} is plotted as a function of the pulse repetition frequency f ($=1/T$), thus highlighting the strong influence of the pulse rate.
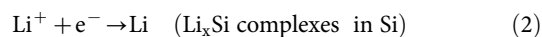
R_{OFF} to the R_{ON} state, as a function of the number of bias pulses applied, *for different top electrode sizes*. As illustrated in Figure 2, the number of pulses required for the resistance decrease depends dramatically on the top electrode surface area. The smallest MIM cells exhibit a higher rate of decrease in resistance -reflecting the reaction kinetics- than the largest cells. This indicates that some volume fraction is involved in the RS process. In addition, preliminary studies on 500 nm wide $M/Li_xCoO_2/M$ cells show, after a very long bias application time, an increase in conductivity of the film surface surrounding the top electrodes (see Supplementary Information S1), which appears compatible with homogeneous RS.

The $Au/Li_xCoO_2/Si$ configuration –not symmetric[22]- of our cells involves Si as the bottom electrode: it corresponds to a solid state microbattery already reported by Ariel *et al*[23] for which, unlike the present study, no RS was observed, possibly due to their specific Li stoichiometry, x. In this case, when the bottom Si electrode is negatively polarized, Li^+ ions migrate towards the doped Si electrode, where they are reduced by forming Li_xSi complexes, thus yielding an electromotive force (EMF). The SiO_2 interface layer (thickness $\geq$ 9 nm, grown by thermal oxidation before Li_xCoO_2 deposition) behaves as a solid state electrolyte allowing Li^+ ion diffusion, while preventing electrical short circuit between the electrodes. While looking for the existence of such a SiO_2 electrolyte layer in our MIM cells, we found that just after the deposition of Li_xCoO_2 film on Si, the Li_xCoO_2/Si interface consists of a 2–3 nm thick native SiO_2 layer, which is considered to be too thin to avoid short circuiting. However, after the required post-annealing step (see Methods), we found that the SiO_2 thickness increased up to almost 17 nm, as confirmed by Transmission Electron Microscopy (TEM) and X-ray Photoelectron Spectroscopy (XPS) (see Supplementary Information S2 and S3).

In order to illustrate the occurrence of an EMF in our "nanobattery", we applied a bias voltage on a MIM cell over a few minutes with the Si electrode being negatively polarized. This resulted, after bias removal, in an induced voltage, as evidenced by I–V curves using slow sweeping voltage rates (see Supplementary Information S4). Such a voltage is attributed to an EMF, and has been studied as a function of the applied bias duration. As illustrated in Fig. 3a, a negative bottom-top bias of −6 V leads first to a rapid decrease of the MIM cell resistance, corresponding to RS from R_{OFF} to R_{ON} (blue curve in Fig. 3a) and it is followed after several minutes, by a progressive increase of the EMF value, reaching about 400 mV after 30
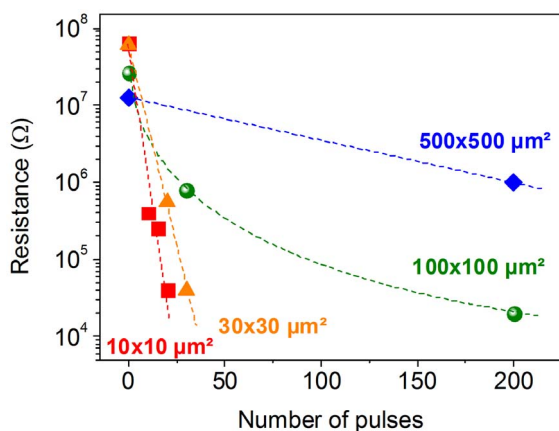

Figure 2 | MIM cell resistance as a function of the number of sequential applied voltage pulses, for different upper electrode surfaces. The MIM cell resistance is plotted as a function of the number of −8 V pulses (τ = 50 ms, T = 150 ms), for various top electrode areas, from 500 $\times$ 500 μm² down to 10 $\times$ 10 μm² (dotted lines are a guide to the eye). The resistance compliance is low enough (10^3–10^4 Ω) to avoid any capacitive effects.

minutes (red curve in Fig. 3a). Such a value, (independent of the top electrode area), is exceptionally high among EMF values reported for VCM cells[18]. Interestingly for our Li_xCoO_2 MIM cells (involving alkali-metal ion redox reactions), the EMF is observed to arise *after* the R_{ON} state is achieved, which underlines an opposite, complementary behavior, compared to electrochemical metallization memory (ECM) systems[24], or VCM systems involving oxygen ion related reactions[18]. Furthermore, we observed that this EMF spontaneously decreases over a few minutes (see red curve in Fig. 3b), while the cell resistance remains surprisingly at its low resistance state R_{ON} ($\cong 10^4$ Ω, blue curve in Fig. 3b). Such a discharge time also confirms the electrochemical nature of the cell voltage. Indeed, the corresponding dielectric discharge time (which is roughly estimated in the 10^{-5} s range) of the cell (with C in the 10^{-9} F range) is seven orders of magnitude lower than the measured discharge time, ruling out any capacitive effects.

For the MIM cells, these observations lead us to propose a cobalt redox reaction involving lithium. For a negative silicon electrode polarization, cobalt is oxidized and lithium is reduced in silicon, as follows:

$$Co^{3+} \rightarrow Co^{4+} + e^- \qquad (1)$$

$$Li^+ + e^- \rightarrow Li \quad (Li_xSi \text{ complexes in Si}) \qquad (2)$$

Although the whole phase diagram of the Li_xCoO_2 system is complex[25], the reported structure of Li_xCoO_2 in the field of batteries allows a qualitative insight on the RS of the MIM cells. For x $\geq$ 0.94, Li_xCoO_2 is considered as a band insulator, whereas for x $\leq$ 0.75, it is a metal. In between, the metallic and insulating phases coexist[26,27]. This phase coexistence most likely occurs through the formation of puddles, like in another correlated oxide, such as V_2O_3 (ref. 28). A global x decrease is associated to the evolution of these coexisting phases: the metal-conducting phase (x $\approx$ 0.75), progressively dominates over the insulating one (x $\approx$ 0.94), corresponding to an insulator-to-metal transition. In our MIM cells, the pristine Li stoichiometry x of Li_xCoO_2 has been determined by X-ray Diffraction measurements to be x $\approx$ 0.95 (with the Co^{3+} concentration being almost constant throughout the film thickness, see Supplementary Information S5). A negative Si polarization leads to the oxidation of Co (which corresponds to equation (1)), and also to the migration of Li^+ ions into the Si electrode (where they are reduced, corresponding to equation (2)), with a consequent decrease of x in the film. The RS from R_{OFF} to R_{ON} (see blue curve in Fig. 3a) can thus be related to the growth of metal-like puddles in the film bulk, ultimately connecting the top and bottom surfaces of the film. It is noted that Ariel *et al.* did not observe RS in their batteries, which can be accounted for by their pristine stoichiometry x = 0.7. Further negative voltage application, during a much longer time (in the minutes range) yields a progressive occurrence of an EMF (red curve in Fig. 3a), which reflects the accumulation of Li in Si, and can be associated to a further x decrease in the Li_xCoO_2 film.

After bias voltage application removal, the EMF spontaneously completely discharges, which reflects Li reinsertion in the Li_xCoO_2 film and thus an x increase. However, this should lead to a recovery of the initial cell resistance. In contrast, at room temperature it remains at its R_{ON} value ($\sim 10^4$ Ω). In our case, switching from the R_{ON} to the R_{OFF} state can be, nevertheless, achieved by the application of a positive bottom-top bias ($\geq$+2 V) (ref 15). In addition, we have observed that this switching recovery from R_{ON} to R_{OFF} can also be induced by heating (see Supplementary Information S6). This R_{ON} stability after the EMF discharge might be correlated to an electrochemical phenomenon already observed in Li_xCoO_2 electrochemical cells involving electrodes different from Si[29], which is attributed to the fact that it is difficult to re-intercalate all the extracted lithium ions[30]. Another possibility, from a physical point
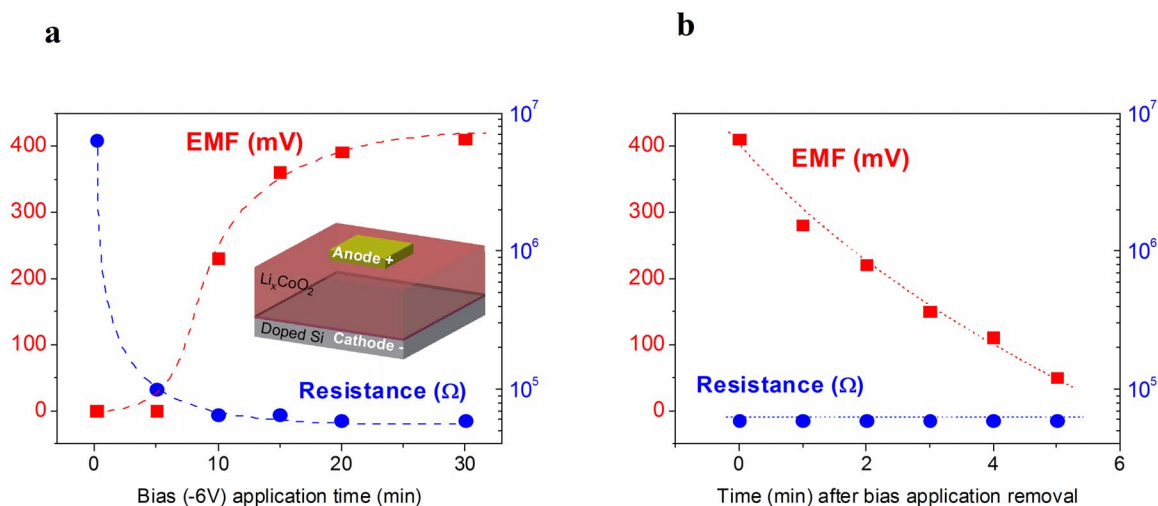
Figure 3 | Evolution, for an MIM cell, of the EMF and the cell resistance, during bias application, and after bias application removal. (a) Evolution of the EMF and the MIM cell resistance, as functions of the applied voltage duration. The inset shows a schematic diagram of the MIM configuration (b) After the bottom/top electrode bias application has been removed, the values of the EMF and MIM cell resistance have been recorded as functions of time. The EMF decreases spontaneously over a few minutes, but the resistance stays at its R_{ON} state.

of view, is that energy must be supplied to some Li^+ ions which may be trapped in the SiO_2 layer, to reinsert them all in the Li_xCoO_2 film. On the other hand, our RS proposed mechanism leaves an open question about the pulse rate dependence, which cannot be linked to the onset of the EMF, since the time scales of the pulse frequency and the EMF are clearly different. This dynamic aspect of the involved process is being actively investigated.

In an effort to better understand the origin of the RS mechanism, we considered a CP-AFM/Li_xCoO_2 direct nanometric contact, which enables us to focus on the changes in the Li_xCoO_2 film alone. In contrast to the MIM cells, a direct {(CP)AFM tip/Li_xCoO_2 surface} contact leads to opposite polarity modifications. For example, as shown in Fig. 4b, a sample-to-probe bias of -8 V results in a large surface conductivity decrease, whereas a MIM cell, in its pristine state, switches to a state (R_{ON}) which is several orders of magnitude more conducting, for the same applied bias voltage (Fig. 4a).

Such opposite switching polarity behavior already suggests a different mechanism. Nevertheless, in order to gain further insight we shall try to identify the specific electrochemical processes involved. Therefore, we investigated the influence of the ambient water vapor pressure (P_{H2O}) on the change of surface conductivity. In the tip-surface case, a water meniscus exists at the interface at ambient air. Its size, which strongly depends on the relative humidity (RH) and thus on the water vapor pressure P_{H2O} (ref. 31), is critical for conducting-probe-mediated electrochemical reactions[32]. As shown in Fig. 5a, at $P_{H2O} = 4$ Torr, surface conductivity can be easily tuned: more (less) conducting areas are obtained after scanning rectangular regions at a $+8$ V (-8 V) sample-tip bias. Using the same procedure, a lower
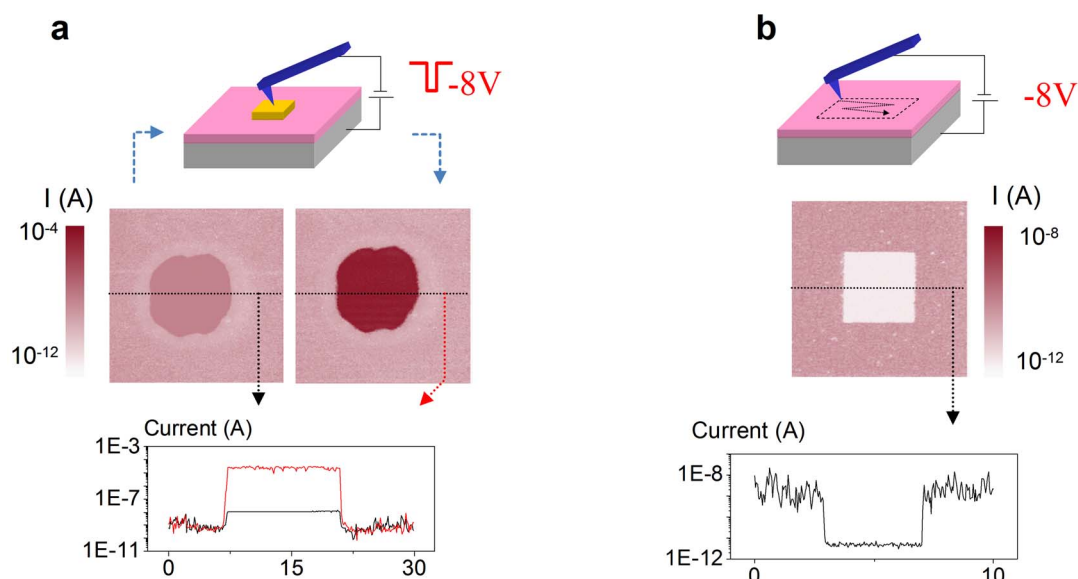

Figure 4 | Comparison of the two investigated configurations: micrometric MIM cell and (CP) AFM tip/surface nanocontact (a) Schematic diagram of a MIM cell, and below, current image of the surface (on top and around a $\sim$10 × 10 µm² upper electrode) scanned with a (CP) AFM tip (at +1 V) before (left) and after (right) applying a pulse of -8 V for 1 s between the lower/upper electrodes; in the corresponding profiles, the cell conductance is 10⁴ times higher after the pulse (in red). (b) Schematic diagram of the tip scanning the film surface, and below, 10 × 10 µm² current image recorded at +1 V following a 4 × 4 µm² scan at -8 V. In the corresponding profile, the conductivity of the modified region has decreased by > 10³ times.
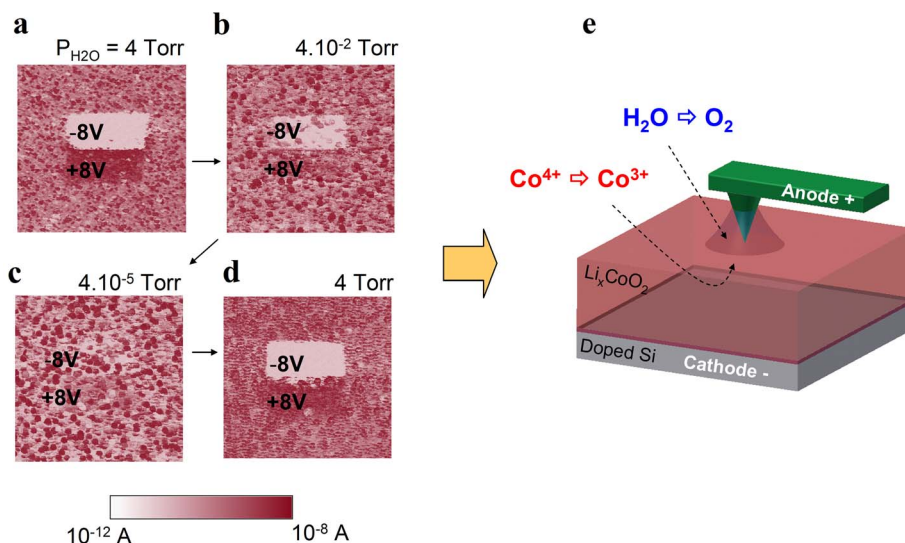
Figure 5 | Electrical images, showing the evolution of the surface-conductivity of Li_xCoO_2 films, as a function of the ambient water vapor pressure, and schematic diagram of the proposed electrochemical reactions occurring in a (CP)AFM probe/film contact, (a), (b), (c), (d) (CP) AFM images from a $10 \times 10\ \mu m^2$ region recorded with $+1$ V after scanning an area of $4 \times 2\ \mu m^2$ with two different sample-tip biases of $+8$ V and -8 V, resulting in surface-conductivity modifications of the Li_xCoO_2 film surface; the influence of the water vapor pressure P_{H2O} on the conductivity modifications is shown in (a, b and c). For $P_{H2O} = 4 \times 10^{-5}$ Torr, almost no modification is distinguishable as shown in (c). When P_{H2O} is increased back to 4 Torr, the surface-conductivity can be tuned again as shown in (d). (e) Schematic diagram of the mechanism proposed for the tip-sample configuration. The condensation water capillary meniscus forms an electrochemical cell; assuming the lower Si electrode is negatively polarized, water is oxidized and cobalt is reduced, yielding a less conducting film surface.

P_{H2O} (4.10^{-2} Torr) yields weaker modifications (Fig. 5b), and at $P_{H2O} = 4 \times 10^{-5}$ Torr, no conductivity modulation can be achieved (Fig. 5c). Increasing P_{H2O} back to 4 Torr, allows sharp conductivity tuning again (Fig. 5d). Under ambient air (60% RH at 25°C, thus $P_{H2O} = 14$ Torr), conductivity modifications even extend to a much larger area than the scanned area (see Supplementary Information S7). These results attest to the kind of involved reactions we previously suggested[15,33], i.e., local cobalt redox reaction, coupled to the meniscus water redox reaction (illustrated in Fig. 5e). The reactions can be written as follows, for a lower-electrode negative polarization:

$$Co^{4+} + e^- \rightarrow Co^{3+} \tag{3}$$

$$H_2O \rightarrow \tfrac{1}{2}\,O_2 + 2H^+ + 2e^- \tag{4}$$
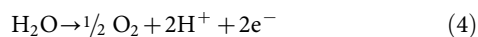
At this point, it is worth noting that a tip-surface contact without water meniscus should yield similar results to MIM cells. However, we did not observe any resistance changes (see Fig. 5c) in this case. This underlines that a (CP) AFM tip cannot be considered as a simple smaller electrode[34]. In the tip-surface configuration, the contact size is in the nm range, much smaller than the film thickness. Therefore, the potential drop is almost concentrated at the tip-surface neighborhood. Hence, the lower doped Si electrode may be ignored, while it is of crucial importance in MIM cells with larger upper electrode surfaces. Thus, the MIM cell configuration and the AFM probe/surface nanocontact both involve Co redox reactions, but the complementary reactions are clearly different (involving lithium in the first case, water in the second).

Discussion

We have observed memristive behaviors in Li_xCoO_2 films, combining the possibilities of multilevel information stacking and biological synapse plasticity emulation. In addition, we have identified the underlying electrochemical reactions inducing RS. Specifically, in the MIM cells, the cobalt redox reaction, which is connected to an insulator-to-metal transition, is coupled to the lithium intercalation/

deintercalation in the conducting silicon electrode, whereas in the (CP) AFM probe-film case, it is coupled to the water redox reaction. Furthermore, we have observed a progressive occurrence of an EMF –more specific of a neuron- in MIM devices, which *follows* the switching from R_{OFF} to R_{ON} state, and disappears *before* the metal-to-insulator reverse transition. This latter transition is not spontaneous, but is induced by applying either voltage or heating. This specific behavior, observed for the first time in Li_xCoO_2 thin film-based MIM solid-state cells, brings together a new combination of possibilities with a potential easy integration on Si-based devices, hence offering exciting new perspectives in nanoelectronics and neuromorphic implementation.

Methods

5

tures (up to 190°C). PtSi tips, as well as conducting diamond coated Si tips were used (spring constant ≈ 2 N/m).

Cross-sectional TEM studies at higher magnification were carried out on Li_xCoO_2 samples using a JEOL 2011 transmission electron microscope working at 200 kV. The samples were prepared by mechanical grinding, followed by ion milling using a GATAN Precision Ion Polishing system.

XPS measurements have been performed using a PHI 5000 Versaprobe spectrometer (Physical Electronics) operating at a base pressure of 1×10^{-7} Pa. A focused monochromatized Al K_α X-ray source (hν = 1486.6 eV) was used at 15 kV. High resolution core level spectra were acquired with a 23.5 eV pass energy, an energy step of 0.1 eV and a 50 ms dwell time. The spectrometer was calibrated with Cu $2p_{3/2}$ and Cu LMM of clean copper at 932.7 eV and 918.7 eV respectively. The Ar ion beam conditions for depth profiling were as follows: Ar ion source was operated at 2 kV and the raster area was 2×2 mm^2. Each sputter cycle was set to 30 s, which corresponds to a sputter depth of 2.6 nm in SiO_2.

1. Waser, R. & Aono, M. Nanoionics-based resistive switching memories. *Nature Mater.* **6**, 833–840 (2007).
2. Sawa, A. Resistive switching in transition metal oxides. *Mater. Today* **11**, 28–36 (2008).
3. Ha, S. D. & Ramanathan, S. Adaptative oxide electronics: A review. *J. Applied Phys.* **110**, 071101 (2011).
4. Waser, R., Dittmann, R., Staikov, G. & Szot, K. Redox-based resistive switching memories — nanoionic mechanism, prospects and challenges. *Adv. Mater.* **21**, 2632–2663 (2009).
5. Strukov, D. B., Snider, G. S., Stewart, D. R. & Williams, R. S. The missing memristor found. *Nature* **453**, 80–83 (2008).
6. Rozenberg, M. J. Resistive switching. *Scholarpedia* **6**, 11414 (2011).
7. Snider, G. S. Spike-timing-dependent learning in memristive nanodevices. Paper presented at *IEEE International Symposium on Nanoscale Architectures*, Anaheim, USA, Publisher: IEEE, DOI: 10.1109/NANOARCH.2008.4585796 (12–13 June 2008).
8. Jo, S.-H. *et al.* Nanoscale memristor device as synapse in neuromorphic systems. *Nano Lett.* **19**, 1297–1301 (2010).
9. Ohno, T. *et al.* Short-term plasticity and long-term potentiation mimicked in single inorganic synapses. *Nature Mater.* **10**, 591–595 (2011).
10. Ziegler, M. *et al.* An electronic version of Pavlov's dog. *Adv. Funct. Mater.* **22**, 2744–2749 (2012).
11. Shi, J., Ha, S. D., Zhou, Y., Schoofs, F. & Ramanathan, S. A correlated nickelate synaptic transistor. *Nature Commun.* **4**, 2676 doi: 10.1038/ncomms3676 (2013).
12. Seo, K. *et al.* Analog memory and spike-dependent plasticity characteristics of a nanoscale titanium oxide bilayer resistive switching device. *Nanotechnol.* **22**, 245023 (2011).
13. Chang, T., Jo, S.-H. & Lu, W. Short-term memory to long-term memory transition in a nanoscale memristor. *ACS Nano* **9**, 7669–7676 (2011).
14. Kuzum, D., Jeyasingh, G. D., Lee, B. & Philip Wong, H. S. Nanoelectronic programmable synapses based on phase change materials for brain-inspired computing. *Nano Lett.* **12**, 2179–2186 (2012).
15. Moradpour, A. *et al.* Resistive switching phenomena in Li_xCoO_2 thin films. *Adv. Mater.* **23**, 4141–4145 (2011).
16. Alberts, B., Johnson, A., Lewis, J. & Raff, M. *Molecular biology of the cell* (Garland Science, 2008).
17. Markram, H., Gupta, A., Uziel, A., Wang, Y. & Tsodyks, M. Information processing with frequency-dependent synaptic connections. *Neurobiology of learning and memory* **70**, 101–112 (1998).
18. Valov, I. *et al.* Nanobatteries in redox-based resistive switches require extension of memristor theory. *Nature Commun.* **4**, 1771 doi: 10.1038/ncomms2784 (2013).
19. Ghenzy, N. *et al.* Optimization of resistive switching performance of metal-manganite oxide interfaces by multipulse protocol. *J. Applied Phys.* **111**, 084512 (2012).
20. Dittmann, R. *et al.* Scaling potential of local redox processes in memristive $SrTiO_3$ thin film devices. *Proc. IEEE* **100**, 1979–1990 (2012).
21. Huang, C. H. *et al.* Manipulated tranformation of filamentary and homogeneous resistive switching on ZnO thin film memristor with controllable multistate. *ACS Appl. Mater. Interfaces* **5**, 6017–6023 (2013).
22. Zhu, X. *et al.* Direct observation of lithium-ion transport under an electrical field in Li_xCoO_2 nanograins. *Sci. Rep.* **3**, 1084 (2013).
23. Ariel, N., Ceder, G., Sadoway, D. R. & Fitzgerald, E. A. Electrochemically control transport of lithium through ultrathin SiO_2. *J. Appl. Phys.* **98**, 023516 (2005).
24. Tappertzhofen, S. *et al.* Generic relevance of counter charges for cation-based nanoscale resistive switching memories. *ACS Nano* **7**, 6396 (2013).
25. Motohaschi, T. *et al.* Electronic phase diagram of the layered cobalt oxide system Li_xCoO_2 (0.0 ≤ x ≤ 1.0). *Phys. Rev. B* **80**, 165114 (2009).
26. Ménétrier, M., Saadoune, I., Levasseur, S. & Delmas, C. The insulator-metal transition upon lithium deintercalation from $LiCoO_2$: electronic properties and ^{7}Li NMR study. *J. Mat. Chem.* **9**, 1135–1140 (1999).
27. Reimers, J. N. & Dahn, J. R. Electrochemical and in situ X-ray diffraction studies of lithium intercalation in Li_xCoO_2. *J. Electrochem. Soc.* **139**, 2091 (1992).
28. Lupi, S. *et al.* A microscopic view on the Mott transition in chromium-doped V_2O_3. *Nature Comm.* **1**,105 doi: 10.1038/nscomms1109 (2010).
29. Nishizawa, M., Yamamura, S., Itoh, T. & Uchida, I. Irreversible conductivity change of $Li_{1-x}CoO_2$ on electrochemical lithium insertion/extraction, desirable for battery applications. *Chem. Commun.* **16**, 1631–1632 (1998).
30. Levasseur, S., Ménétrier, M., Suard, E. & Delmas, C. Evidence for structural defects in non-stoichiometric HT-$LiCoO_2$: electrochemical, electronic properties and ^{7}Li NMR studies. *Solid State Ionics* **128**, 11–24 (2000).
31. Weeks, B. L., Vaughn, M. W. & DeYoreo, J. J. Direct Imaging of Meniscus Formation in Atomic Force Microscopy Using Environmental Scanning Electron Microscopy. *Langmuir* **21**, 8096–8098 (2005).
32. Li, Y., Maynor, B. W. & Liu, J. Electrochemical AFM "Dip-Pen" nanolithography. *J. Am. Chem. Soc.* **123**, 2105–2106 (2001).
33. Schneegans, O. *et al.* Na_xCoO_2: A new opportunity for rewritable media? *J. Am. Chem. Soc.* **108**, 9882 (2007).
34. Lee, M. H. & Hwang, C. S. Resistive switching memory: observations with scanning probe microscopy. *Nanoscale* **3**, 490–502 (2011).

Acknowledgments

Author contributions

R.S. synthesized the films; P.A.S., T.M., G.A. and R.W. fabricated the devices, V.H.M. performed the film modifications by (CP) AFM; J.G., C.N.M., C.M.O., E.S., A.B., C.B.L., P.A.A., K.W., F.J., D.A. and K.M. performed the film characterizations; All authors (including S.F., A.R., P.L., P.A. and P.C.) extensively discussed the results; the paper was written by O.S. with the help of A.M., C.P., J.G. and M.J.R.

Additional information

Supplementary information accompanies this paper at http://www.nature.com/scientificreports

Competing financial interests: The authors declare no competing financial interests.

How to cite this article: Mai, V.H. *et al.* Memristive and neuromorphic behavior in a Li_xCoO_2 nanobattery. *Sci. Rep.* **5**, 7761; DOI:10.1038/srep07761 (2015).